Simulations of Near-Field Intensity Modulations in High-Intensity Laser Beams due to Self- and Cross-Phase Modulation Between Orthogonally Polarized Laser Beams Emerging from a Diamond-Turned KDP Wedge

The near-field intensity modulation due to a diamond-turned KDP wedge is investigated through computer simulations within the framework of its application to LLE's OMEGA laser system. KDP wedges will be installed on each OMEGA beamline and mounted 12 m away from the final focusing optics. The wedges will improve the direct-drive inertial confinement fusion uniformity by a process known as polarization smoothing. Diamond turning is the finishing process of choice due to the greater cost incurred by installing polished KDP crystals on every beamline.

The Nova laser facility at the Lawrence Livermore National Laboratory (LLNL) reported blast-shield damage that was linked to the mid-range spatial wavelengths (1 to 4 mm) of scratch marks on diamond-turned KDP crystals in use at the time. This motivated LLE to employ polished KDP crystals for frequency tripling on OMEGA during its 24- to 60-beam upgrade (completed in 1995) because polishing produces a smoother distribution of spatial wavelengths of lower amplitude. While diamond-turning technology has improved recently, residual concern has existed regarding the potential damaging effects of installing diamond-turned KDP crystals. This has prompted an investigation, both theoretical and experimental, into the potential effects of the scratch or milling marks left behind by diamond turning.

This article represents part of the theoretical investigation of this problem. In particular, the simulations model the nonlinear effects that result from (1) the beam propagation through the 12 m of air that separates the KDP wedge from the final focusing optics, (2) the initial phase perturbation of the beam due to the residual scratch marks on the diamond-turned KDP surface, and (3) the nonlinear index's polarization dependence. The danger here is that small-scale self-focusing might develop high-intensity spikes leading to filamentation damage in the final focusing optics. The simulations reported here demonstrate that KDP wedges, diamond-turned or smooth, are not a significant source of intensity modulation under OMEGA laser conditions. In addition, for a beam with a varying polarization state, these simulations exhibit an intensity enhancement in the vicinity of linear polarization due to the nonlinear effect of cross-phase modulation.

Diamond-Turned KDP Wedge

1. Polarization Smoothing

The concept of polarization smoothing originated from Kato[1] who recognized the uniformity that would result from rotating the polarization through 90° on half of the individual phase-plate elements chosen at random. A more practical device, first described in Ref. 2, is a wedge of birefringent material such as KDP. A linearly polarized beam incident upon the KDP wedge is split into two orthogonally polarized beams of equal intensity when the incident beam's polarization vector is oriented at 45° with respect to the slow and fast axes of the crystal (see Fig. 76.27). The resultant two orthogonal beams co-propagate at a slight angle of separation with respect to each other, determined by the wedge angle and the refractive indexes for the slow and fast waves. The current requirements for OMEGA set the wedge angle to 4.5 min. This causes a separation angle of 44 μrad between the two orthogonal beams and a relative offset of 80 μm after focusing on target. The relative offset of 80 μm achieves an instantaneous theoretical $1/\sqrt{2}$ reduction of the nonuniformity through spatial averaging, which complements the uniformity achieved by SSD alone.[3]

As a consequence of the separation angle, the combined polarization state of the two orthogonally polarized beams continuously cycles through all elliptical states along any transverse plane. The rate of change is determined by the transverse components of the wave vectors. Since the separation angle is small, the wavelength of the cycle is given by

$$\lambda_{\text{pol}} = \frac{\lambda}{\sin(\theta)} = \frac{351\ \text{nm}}{\sin\left(44\ \mu\text{rad}\right)} = 8\ \text{mm}, \qquad (1)$$

where $\lambda = 351$ nm is the UV operating wavelength of OMEGA. The resultant $\lambda_{\text{pol}} = 8$ mm is the transverse distance required to cycle the polarization state from right-handed circular, to

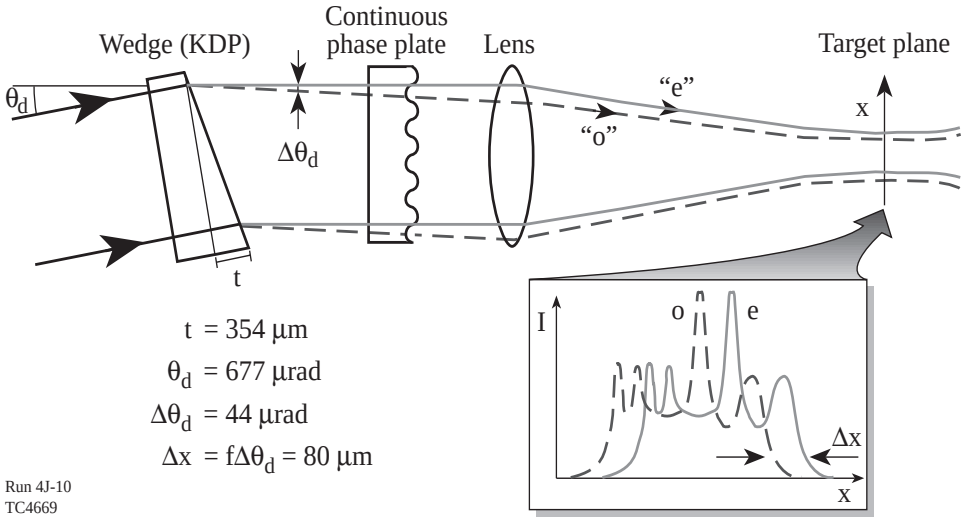

Figure 76.27
A birefringent KDP wedge achieves polarization smoothing and a theoretical $1/\sqrt{2}$ reduction in nonuniformity.

linear, to left-handed circular, back to linear, and returning to right-handed circular.

2. Induced Phase Perturbations

Two types of phase perturbation result from the introduction of a diamond-turned KDP wedge. The first is due to the residual scratch marks left behind by the diamond-turning process. The scratch marks cause a beam to acquire a pseudorandom phase perturbation as the beam passes through the front and back faces of the crystal. The pseudorandom phase perturbation can be described by a thin-optic transformation

$$\Phi_{\text{mill}} = k_0\left(n_{\text{KDP}} - 1\right) S(y), \tag{2}$$

where $S(y)$ is the depth of the scratch mark as a function of the transverse position y, $k_0 \equiv 2\pi/\lambda$ is the vacuum wave number, and n_{KDP} represents the refractive index for either the slow or fast wave.

The second type of phase perturbation arises during propagation because the nonlinear refractive index is a function of polarization state and intensity (see subsection 1 of the **Ellipticity** section) together with the fact that the KDP wedge produces a beam whose combined polarization state varies as a function of transverse position y. The nonlinear refractive index is a maximum for linear polarization and a minimum for circular polarization. Therefore, both orthogonally polarized beams accumulate a periodic phase perturbation during propagation that is greatest in the vicinity of linear polarization.

Both types of phase perturbation affect the beams by introducing spatial phase modulation that can then be converted into intensity modulation by virtue of the diffractive process that occurs during propagation. Intense beams can develop high-intensity spikes leading to filamentation damage through the coupled process of phase modulation and diffraction.

3. Model of Scratch Marks

The pseudorandom behavior of the residual scratch marks is modeled in this article by bandpass filtering a white noise source, viz.

$$S(y) = F^{-1}\left\{F\left[\Xi(y)\right] \bullet \text{rect}\left(\frac{k_y - k_{y_0}}{k_{y_{\max}} - k_{y_{\min}}}\right)\right\},$$

$$\text{rect}(x) = \begin{cases} 1; & |x| \le \dfrac{1}{2} \\ 0; & |x| > \dfrac{1}{2} \end{cases}, \tag{3}$$

where F represents the spatial Fourier transform, $\Xi(y)$ is the noise source, k_{y_0} is the central spatial wave number, and $k_{y_{\max}}$ and $k_{y_{\min}}$ represent the maximum and minimum passed spatial wave numbers. This result is sometimes referred to as "colored" noise.[4] Figure 76.28 illustrates an example in which the passband was set to $2\pi/(4\text{ mm}) \le k_y \le 2\pi/(2\text{ mm})$. These data are used in the subsequent illustrative numerical simulations given in the **Numerical Results** section. This passband was selected since it covers the troublesome spatial frequencies identified by LLNL. Also, these data closely resemble surface profile measurements on a qualitative basis. An alternative function that completely describes the power spectral density of the scratch marks could be used in place of the

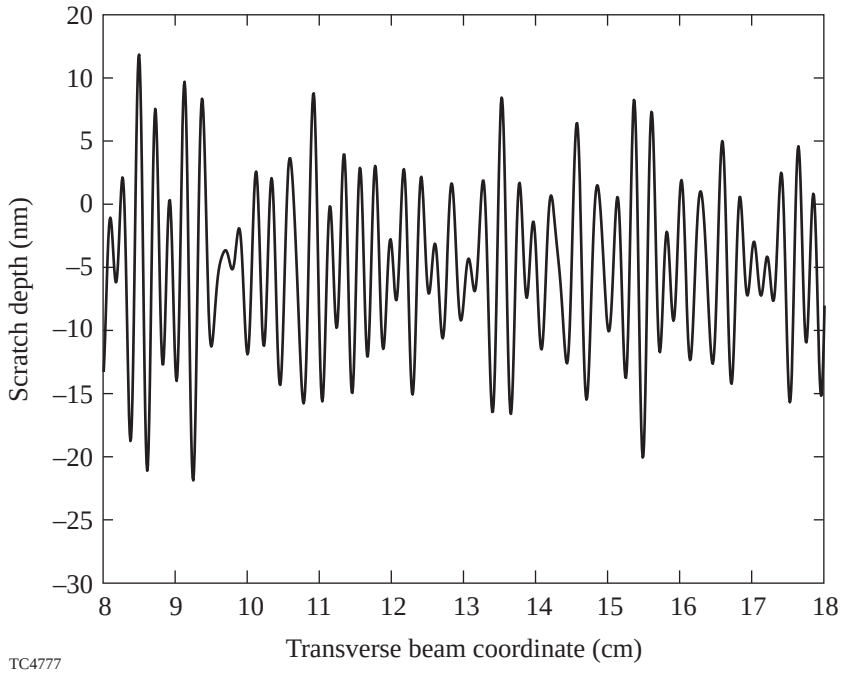

Figure 76.28
A bandpass-filtered pseudorandom noise source where the passband is set to $2\pi/(4\text{ mm}) \le k_y \le 2\pi/(2\text{ mm})$ and the peak-to-valley scratch depth is 40 nm.

rect(k_y) function. However, an adequate statistical description of the diamond-turned scratch marks is unavailable at this time. The rect(k_y) can be viewed as a worse-case situation that emphasizes the higher spatial frequencies since the actual power spectral density would go to zero in a continuous manner as the spatial frequency increases.

Nonlinear Wave Equation

The analysis of beam propagation for this problem assumes that the optical field is monochromatic and the bandwidth of the spatial spectrum is small relative to the vacuum wave number $k_0 = \omega_0/c$, where ω_0 is the angular frequency and c is the vacuum speed of light. This permits the slowly varying amplitude to be separated from the rapidly varying part, such that the electric field vector is given by

$$\mathbf{E}(y,z,t) = \frac{1}{2}\left[\hat{\mathbf{p}}E(y,z)\,e^{-i(\omega_0 t - k_0 n_0 z)} + c.c.\right], \qquad (4)$$

where $E(y,z)$ is the slowly varying complex amplitude as a function of both the transverse distance y and propagation distance z, $\hat{\mathbf{p}}$ is the polarization vector, n_0 is the refractive index, and *c.c.* indicates the complex conjugate. An arbitrary elliptical polarization state decomposes naturally into a weighted vector sum of right-handed and left-handed circular polarization states, viz.

$$\begin{aligned}\mathbf{E}(y,z,t) &= \frac{1}{2}\left\{\left[\hat{\mathbf{p}}_{\mathrm{RH}}E_{\mathrm{RH}}(y,z) + \hat{\mathbf{p}}_{\mathrm{LH}}E_{\mathrm{LH}}(y,z)\right]e^{-i(\omega_0 t - k_0 n_0 z)}\right. \\ &\quad \left. + \ c.c.\right\}, \end{aligned} \qquad (5)$$

where $E_{\mathrm{RH}}(y,z)$ and $E_{\mathrm{LH}}(y,z)$ are the complex amplitudes of the right-handed and left-handed circular polarization states, which are defined in terms of Cartesian components as

$$\begin{aligned} E_{\mathrm{RH}}(y,z) &= \frac{1}{\sqrt{2}}\left[E_x(y,z) - E_y(y,z)\right], \\ E_{\mathrm{LH}}(y,z) &= \frac{1}{\sqrt{2}}\left[E_x(y,z) + E_y(y,z)\right], \end{aligned} \qquad (6)$$

and the polarization vectors are defined as

$$\hat{\mathbf{p}}_{\mathrm{RH}} \equiv \frac{1}{\sqrt{2}}\left(\hat{\mathbf{x}} + i\hat{\mathbf{y}}\right), \qquad \hat{\mathbf{p}}_{\mathrm{LH}} \equiv \frac{1}{\sqrt{2}}\left(\hat{\mathbf{x}} - i\hat{\mathbf{y}}\right). \qquad (7)$$

The optical field is assumed to propagate in a lossless, isotropic nonlinear Kerr-like medium, where the nonlinear refractive index is given by

$$n = n_0 + \Delta n. \tag{8}$$

The quantity Δn represents the change in the refractive index beyond the low-intensity value n_0 and exhibits a linear dependence on the optical field intensity. The scalar nonlinear wave equation for each vector component is then given by

$$\frac{\partial E_{\mathrm{RH}}(y,z)}{\partial z} = \frac{i}{2k}\nabla_T^2 E_{\mathrm{RH}}(y,z) + ik_0\,\Delta n_{\mathrm{RH}}\,E_{\mathrm{RH}}(y,z), \tag{9}$$

$$\frac{\partial E_{\mathrm{LH}}(y,z)}{\partial z} = \frac{i}{2k}\nabla_T^2 E_{\mathrm{LH}}(y,z) + ik_0\,\Delta n_{\mathrm{LH}}\,E_{\mathrm{LH}}(y,z), \tag{10}$$

where $k = k_0 n_0$ and[5]

$$\Delta n_{\mathrm{RH}} = \frac{3}{4n_0}\left[\chi^{(3)}_{xyxy}\left|E_{\mathrm{RH}}(y,z)\right|^2 + \left(\chi^{(3)}_{xyxy} + \chi^{(3)}_{xxyy}\right)\left|E_{\mathrm{LH}}(y,z)\right|^2\right], \tag{11}$$

$$\Delta n_{\mathrm{LH}} = \frac{3}{4n_0}\left[\chi^{(3)}_{xyxy}\left|E_{\mathrm{LH}}(y,z)\right|^2 + \left(\chi^{(3)}_{xyxy} + \chi^{(3)}_{xxyy}\right)\left|E_{\mathrm{RH}}(y,z)\right|^2\right], \tag{12}$$

and it has been assumed that $\partial^2 E(y,z)/\partial z^2 = 0$, i.e., the slowly varying envelope approximation. The first terms in Eqs. (11) and (12) represent self-phase modulation, and the second group of terms represents cross-phase modulation. The vector components are coupled through the cross-phase modulation terms. Due to the symmetry of centrosymmetric Kerr-like media and the fact that both vector components share the same frequency ω_0, there are only two independent third-order susceptibility constants $\chi^{(3)}_{xyxy}$ and $\chi^{(3)}_{xxyy}$ that obey the relation $\chi^{(3)}_{xxxx} = 2\chi^{(3)}_{xyxy} + \chi^{(3)}_{xxyy}$ and follow the frequency convention $\chi^{(3)}_{xyxy}(-\omega,-\omega,\omega,\omega)$. (Notice that it is this convention that causes the subtle notational deviation from that of Sutherland.[5]) Either scalar nonlinear wave equation, Eq. (9) or Eq. (10), can be written in operator form as[6]

$$\frac{\partial E(y,z)}{\partial z} = \left(\hat{D} + \hat{N}\right)E(y,z), \tag{13}$$

where the operator $\hat{D}$ accounts for diffraction and is defined as

$$\hat{D} \equiv \frac{i}{2k}\nabla_T^2, \tag{14}$$

the operator $\hat{N}$ governs media nonlinearities and is defined as

$$\hat{N} \equiv ik_0\Delta n, \tag{15}$$

the quantity $E(y,z)$ represents either the right-handed or left-handed complex amplitude, and Δn represents either Eq. (11) or Eq. (12). The formally exact solution of Eq. (13) is given by

$$E(y, z+\Delta z) = e^{i(\hat{D}+\hat{N})\Delta z}\,E(y,z).$$

An important merit of decomposing an arbitrary elliptical polarization state into right-handed and left-handed circular polarization states is that

$$\frac{\partial\left|E_{\mathrm{RH}}(y,z)\right|^2}{\partial z} = 0 \quad \text{and} \quad \frac{\partial\left|E_{\mathrm{LH}}(y,z)\right|^2}{\partial z} = 0.$$

This implies that the intensities of the vector components and therefore the quantity Δn are all constants of motion. This is not true for a Cartesian decomposition, due to the well-known cross-phase modulation effect of ellipse rotation, which causes the magnitudes along the Cartesian components to change with propagation distance.[7]

1. Ellipticity and the Nonlinear Refractive Index

The ellipticity parameter η covers the range $-\pi/4 \le \eta \le \pi/4$, where $\tan(\eta)$ describes the ratio of the minor and major axes of the polarization ellipse with the sign defining its handedness [positive (+) indicates right-handed and negative (–) indicates left-handed].[7] When $\eta = 0$, the polarization state is linear and, when $|\eta| = \pi/4$, the polarization state is circular. Equations to calculate the lengths of the major and minor axes can be found in Oughstun[8] (see Ref. 8, Sec. 4.2.1) and are governed by the complex amplitudes $E_{\mathrm{RH}}(y,z)$ and $E_{\mathrm{LH}}(y,z)$. Consequently, the ellipticity parameter η is also a function of the complex amplitudes $E_{\mathrm{RH}}(y,z)$ and $E_{\mathrm{LH}}(y,z)$. The quantities Δn_{RH} and Δn_{LH} depend on the magnitudes $\left|E_{\mathrm{RH}}(y,z)\right|$ and $\left|E_{\mathrm{LH}}(y,z)\right|$ and are indirectly functions of the polarization state.

The extrema of the quantities Δn_{RH} and Δn_{LH} occur when the polarization state is either linear or circular. If the polarization state is linear, then $|E_{lin}|^2 = 2|E_{LH}|^2 = 2|E_{RH}|^2$ (where the factor of 2 comes from the equal intensity split into both polarization states), and the change in the nonlinear refractive index becomes

$$\Delta n_{lin} = \frac{3}{8n_0}\left[\chi^{(3)}_{xxyy} + 2\chi^{(3)}_{xyxy}\right]|E_{lin}|^2 . \quad (16)$$

If the polarization state is circular, either right-handed or left-handed, then

$$\Delta n_{cir} = \frac{3}{4n_0}\chi^{(3)}_{xyxy}|E_{cir}|^2 . \quad (17)$$

In either of these two degenerate states $|E_{lin}|^2 = |E_{cir}|^2$ so that

$$\Delta n_{lin} > \Delta n_{cir} . \quad (18)$$

In a more general sense, the nonlinear refractive index is larger in the vicinity surrounding, or in the immediate neighborhood of, the points of linear polarization relative to the minimum values attained at the points of right-handed or left-handed circular polarization.

2. Angular Spectrum Representation

If nonlinear effects can be neglected, the vector components become decoupled and obey the scalar Helmholtz wave equations given by

$$\nabla^2 E(y,z) + k_0^2 n^2 E(y,z) = 0, \quad (19)$$

which has an exact solution at any exit plane $z + \Delta z$ given by the angular spectrum representation (see Ref. 9, Sec. 3.7), viz.

$$E(y, z+\Delta z) = \frac{1}{2}\pi \int_{-\infty}^{\infty} \tilde{E}(k_y, z) e^{i\Delta z\sqrt{k_0^2 n^2 - k_y^2}}\, e^{ik_y y} dk_y , \quad (20)$$

where $\tilde{E}(k_y, z)$ is the spatial Fourier transform at the entrance plane z and is defined by

$$\tilde{E}(k_y, z) = \int_{-\infty}^{\infty} E(y,z) e^{-ik_y y} dy . \quad (21)$$

3. Self- and Cross-Phase Modulation

If diffraction can be neglected, the scalar nonlinear wave equation for either vector component has the simple form

$$\frac{\partial E(y,z)}{\partial z} = \hat{N} E(y,z), \quad (22)$$

which has a solution given by

$$E(y, z+\Delta z) = E(y,z) e^{ik_0 \Delta n \Delta z} , \quad (23)$$

because the quantity Δn is not a function of the propagation distance for a circular-polarization decomposition. As a result, the nonlinear effects of self- and cross-phase modulation, acting alone, induce a simple phase accumulation that is a function of both the polarization state and intensity. This is a generalization of the well-known B-integral.

Numerical Approach

The numerical split-step Fourier method (see Ref. 6, Sec. 2.4.1) is used to solve the differential Eq. (13), where the total required distance of propagation is divided into small steps over which the linear effects of diffraction are treated separately from the nonlinear effects of self- and cross-phase modulation. This permits the solutions given by Eqs. (20) and (23) to be used if the chosen step size is sufficiently small that the linear and nonlinear effects are approximately independent over that step.

The numerical calculation over one small step Δz is referred to as a propagation step. One propagation step entails the independent calculation of diffraction using the results of Eq. (20) and the independent calculation of the nonlinear phase accumulation as described by Eq. (23). The detailed manner in which this is carried out greatly affects the overall error achieved and directly affects the required number of steps needed to obtain a suitable level of accuracy. For example, if a full diffraction step is followed by a full nonlinear step, the error is $O\{\Delta z^2\}$, which is equivalent to solving Eq. (13) as

$$E(y, z+\Delta z) \cong e^{i\Delta z \hat{D}} e^{i\Delta z \hat{N}} E(y,z). \quad (24)$$

However, if a half diffraction step is followed by a full nonlinear step and then by another half diffraction step, the error is $O\{\Delta z^3\}$, which is equivalent to solving Eq. (13) as

$$E(y, z+\Delta z) \cong e^{i\frac{\Delta z}{2}\hat{D}} e^{i\Delta z \hat{N}} e^{i\frac{\Delta z}{2}\hat{D}} E(y,z). \quad (25)$$

The errors associated with Eqs. (24) and (25) are found by comparing these approximate solutions to the formally exact

solution to Eq. (13) and applying the Baker–Hausdorff formula for two noncommuting operators.[6] The method described by Eq. (25), known as the symmetrized split-step Fourier method, is employed for the numerical simulations in the subsequent section. Figure 76.29 graphically represents this particular approach over two small steps of Δz.

Numerical Results

The intent of this investigation is to isolate the effects caused by the nonlinear propagation in air, the scratch marks, and the wedged shape of the KDP crystal, while ignoring the nonlinear index of KDP. To this end, only the exit face of the KDP crystal is considered to be scratched, and the initial beam shape is regarded as infinitely smooth. As a consequence, the nonlinear ripple growth within the KDP crystal can be neglected.

The beam shape is modeled by using spatially offset hyperbolic-tangent step functions, viz.

$$E(y) = \frac{1}{2}\left\{\tanh\left[100(y+0.14)\right] - \tanh\left[100(y-0.14)\right]\right\}, \quad (26)$$

which yields an infinitely smooth, 28-cm-diam beam. The nominal intensity level for OMEGA equal to 1.3 GW/cm^2 is used. Also, an unrealistic value of 10.3 GW/cm^2 is used to demonstrate a regime where the nonlinear effects dominate since, as it will be shown, the nonlinear effects are small for the nominal OMEGA intensity level. The measure of intensity modulation used in this paper is the contrast defined as

$$\text{Contrast} = \frac{\max\{I(y)\}}{\text{mean}\{I(y)\}}, \quad (27)$$

where the transverse position y, for this formula only, covers the region where $I(y)$ was initially at full value; thus, the region where the beam intensity tapers to zero is not considered for this statistic.

1. Material Parameters

The material parameters used in the simulations are given in this subsection. The linear refractive indices for the KDP crystal are $n_{\mathrm{KDP}_o} = 1.532498$ for the ordinary wave and $n_{\mathrm{KDP}_e} = 1.498641$ for the extraordinary wave, which propagates at 59° to the optic axis. The third-order nonlinear susceptibility constants for air are

$$\chi^{(3)}_{xyxy}(-\omega,-\omega,\omega,\omega) = 28.16 \times 10^{-19} \text{ esu}$$

and

$$\chi^{(3)}_{xxyy}(-\omega,-\omega,\omega,\omega) = 172.4 \times 10^{-19} \text{ esu}\cdot$$

The third-order susceptibility constants are four times those given in Ref. 10, due to the particular definitions they used for the polarization vector and intensity, as noted by Sutherland [see Ref. 5, p. 298]. There is a compensatory factor of 1/4 in the definition of Δn used in this article, which effectively balances this deviation.

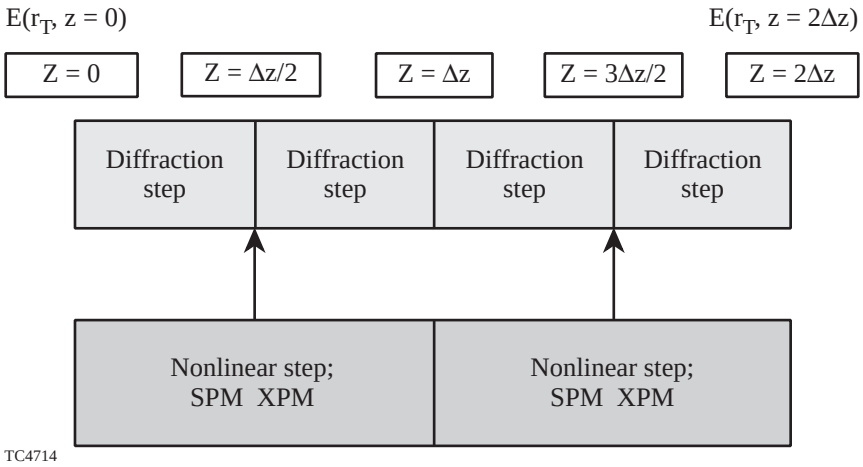

Figure 76.29
Two propagation steps of the symmetrized split-step Fourier method covering a distance of 2Δz.

2. Enhancement of Linear Polarization

As was mentioned in subsection 1 of the **Nonlinear Wave Equation** section, the phase accumulation is greatest in the vicinity surrounding points of linear polarization. When diffraction is included, these areas tend to focus and correspond to peaks of intensity modulation. To illustrate this effect, a simulation was carried out modeling a KDP wedge with an optically smooth surface, i.e., without an initial pseudorandom phase perturbation. Due to the wedge and the dependence of the nonlinear refractive index on the polarization state, a ripple is introduced with a wavelength 1/2 λ_{pol} (where the factor of 1/2 emphasizes that the overall phase perturbation of both orthogonal beams has extrema at the transverse positions corresponding to linear or circular polarization that are independent of the handedness), which can lead to small-scale self-focusing if the beam intensity is high enough. This is contrary to what would be expected in the absence of a wedge; with a perfectly smooth beam and an optically smooth KDP surface, one would observe only a rotation of the polarization ellipse (except in the degenerate cases when the whole beam is either linearly or circularly polarized) and possibly whole-beam self-focusing. This simulation was run with an input intensity of 10.3 GW/cm^2 and yielded a contrast of 1.31. These results are presented in Fig. 76.30, where a correlation between the peak intensities and the linear polarization is evident by the location of the square symbols. If the intensity were lowered to the nominal OMEGA level, a small contrast of only 1.04 would be calculated.

The enhancement of linear polarization may be amplified or seeded by the presence of scratch marks on the surface of the KDP wedge. This effect can be understood by running a simulation that accounts only for diffraction. In this situation there is, of course, no correlation between the intensity peaks that develop during propagation and the polarization state. Some intensity peaks, however, are inevitably located in the neighborhood of linear polarization. These intensity peaks seed the nonlinear growth by increasing the associated phase accumulation in these regions as described by Eq. (23) and, as a consequence, induce a greater intensity modulation than observed for the optically smooth wedge.

A simulation for the nominal OMEGA laser intensity, including both linear and nonlinear effects, yielded a contrast of 1.32 and is presented in Fig. 76.31(a). In this case, only a slight correlation exists between the intensity peaks and the linear polarization state due to the weak nonlinear effect. When the intensity level is increased to 10.3 GW/cm^2, however, an appreciable growth is observed in the vicinity of linear polarization [as shown in Fig. 76.31(b)], and, consequently, a

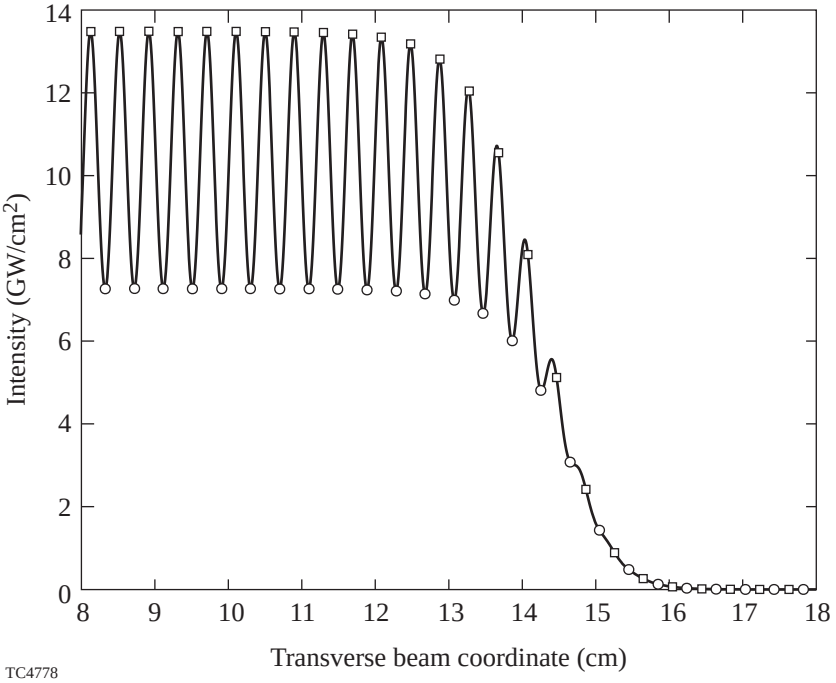

Figure 76.30
The simulation of propagating 12 m past an optically smooth KDP wedge with an incident intensity level of 10.3 GW/cm^2. A contrast of 1.31 is observed. Squares and circles indicate positions of linear and circular polarization, respectively.

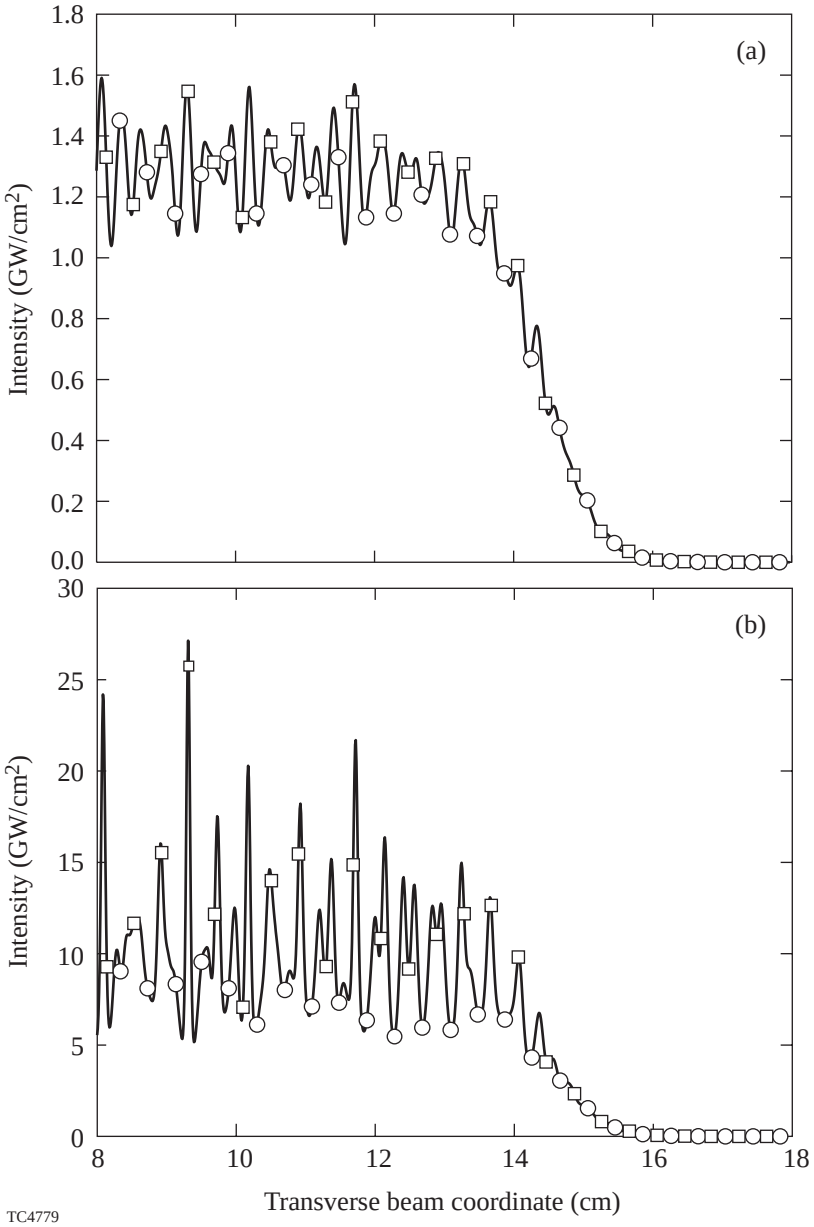

Figure 76.31
The simulation of nonlinear propagation through 12 m of air past a pseudorandomly scratched KDP wedge with 40-nm peak-to-valley scratch depth and a passband of $2\pi/(4\text{ mm}) \le k_y \le 2\pi/(2\text{ mm})$ (a) at 1.3 GW/cm^2 and (b) at 10.3 GW/cm^2. The resulting contrast is 1.32 in (a) and 2.63 in (b). Squares and circles indicate positions of linear and circular polarization, respectively.

significant correlation exists between the intensity peaks and these regions as indicated by the association of the majority of the square symbols with the intensity peaks.

3. Contrast Calculations at the Nominal OMEGA Intensity Level

Tables 76.I and 76.II contain contrast data calculated from simulations of linear and nonlinear propagation, respectively, in which the same scratch-depth data presented in Fig. 76.28 was scaled to cover the 10-nm to 50-nm range for an incident intensity level of 1.3 GW/cm^2. The scratch-depth range presented here was chosen to correspond to the range of surface profile measurements that were taken on diamond-turned KDP crystals, which yielded peak-to-valley scratch depths of 40 nm (worst case) and 15 nm (best case). These tables also include calculated contrast data for three additional passband configurations: the passband is narrowed to $k_y = 2\pi/(3\text{ mm})$, widened to $2\pi/(100\text{ mm}) \le k_y \le 2\pi/(1\text{ mm})$ and widened to a low pass of $k_y \le 2\pi/(1\text{ mm})$.

If the scratch mark model given in Eq. (3) is extended to include another spatial dimension, a 2-D colored noise source is modeled. A 2-D beam is then modeled by extending Eq. (26) to include another dimension. Both of these models are then

used to simulate 2-D nonlinear beam propagation in an analogous manner to the 1-D case. The plot presented in Fig. 76.32 shows three lineouts from a 2-D simulation (taken at the center and near the edges of the beam) for a beam with an intensity of 1.3 GW/cm^2, a scratch-mark passband of $2\pi/(4\text{ mm}) \le k_x, k_y \le 2\pi/(2\text{ mm})$, and a peak-to-valley scratch depth of 40 nm. The contrast calculated for the whole 2-D beam is 1.35, compared to the value of 1.32 given in Table 76.II for the corresponding 1-D case.

At the nominal OMEGA intensity level of 1.3 GW/cm^2, a contrast ratio of 1.8:1 represents the damage threshold of the final optics. The data in Table 76.II show that the calculated contrast values are well below this threshold even for grating-type sinusoidal scratch marks. Recent linear intensity modulation measurements taken on diamond-turned KDP crystals yielded a range of contrast values between 1.04 to 1.08, which roughly correlates with the linear propagation simulation results for peak-to-valley scratch depths between 10 and 20 nm and a passband of $2\pi/(100\text{ mm}) \le k_y \le 2\pi/(1\text{ mm})$ given in Table 76.I. The corresponding contrast range in Table 76.II for nonlinear propagation is 1.07 to 1.11, which represents a small increase due to the nonlinear effects. Near-field images were taken during OMEGA full-power shots on a beamline with and without a diamond-turned KDP plate at an equivalent plane of the final focusing optics. In this experiment, a negligible increase in the intensity modulation was observed, corroborating the results of these numerical simulations.

Conclusion

On the basis of realistic simulations, including diffraction and nonlinear self- and cross-phase modulation, and a realistic representation of scratch marks on diamond-turned KDP, it has been found that KDP wedges, diamond-turned or smooth, are not a significant source of intensity modulation. These results are consistent with experimental results from full-power shots. Accordingly, polarization smoothing will be implemented on OMEGA using diamond-turned rather than polished KDP.

Table 76.I: The calculated value of contrast for linear propagation through 12 m of air past a scratched KDP wedge at an incident intensity level of 1.3 GW/cm^2 for different scratch depths and filter types.

Peak-to-Valley Scratch Depth (nm)	Sinusoidal $k_y = 2\pi/(3\text{ mm})$	Random Lowpass $k_y \le 2\pi/(1\text{ mm})$	Random Bandpass $2\pi/(1\text{ mm}) \le k_y \le 2\pi/(1\text{ mm})$	Random Bandpass $2\pi/(4\text{ mm}) \le k_y \le 2\pi/(2\text{ mm})$
10	1.08	1.03	1.04	1.06
20	1.16	1.07	1.08	1.11
30	1.23	1.11	1.11	1.17
40	1.31	1.14	1.14	1.23
50	1.38	1.18	1.19	1.28

Table 76.II: The calculated value of contrast for nonlinear propagation through 12 m of air past a scratched KDP wedge at an incident intensity level of 1.3 GW/cm^2 for different scratch depths and filter types.

Peak-to-Valley Scratch Depth (nm)	Sinusoidal $k_y = 2\pi/(3\text{ mm})$	Random Lowpass $k_y \le 2\pi/(1\text{ mm})$	Random Bandpass $2\pi/(1\text{ mm}) \le k_y \le 2\pi/(1\text{ mm})$	Random Bandpass $2\pi/(4\text{ mm}) \le k_y \le 2\pi/(2\text{ mm})$
10	1.13	1.07	1.07	1.11
20	1.23	1.09	1.11	1.18
30	1.32	1.13	1.16	1.25
40	1.41	1.17	1.19	1.32
50	1.50	1.20	1.25	1.38

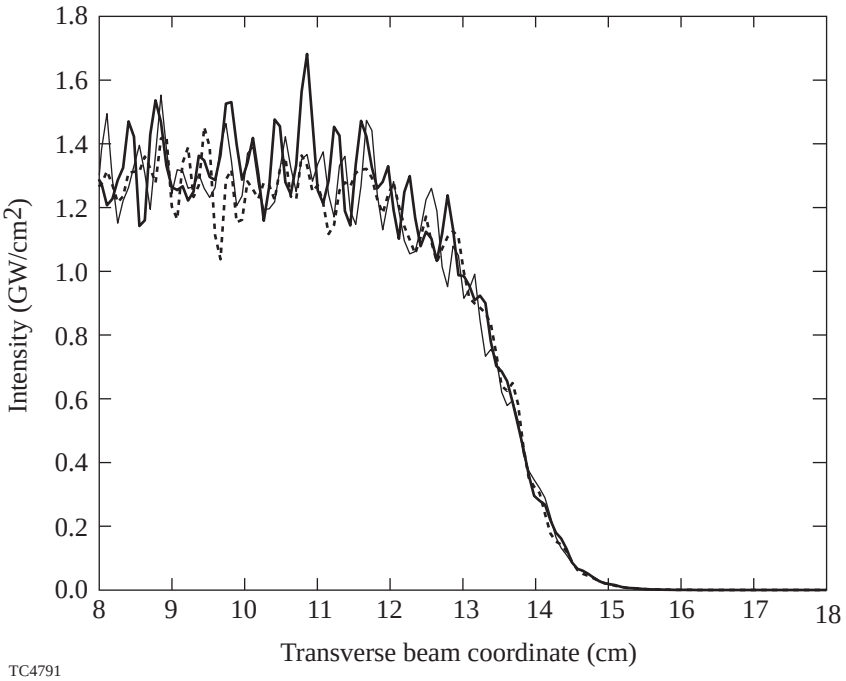

Figure 76.32
Three lineouts from a 2-D simulation (taken at the center and near the edges of the beam) of nonlinear beam propagation with a 1.3 GW/cm^2 intensity, through 12 m of air, past a pseudorandomly scratched KDP wedge with 40-nm peak-to-valley scratch depth and a passband of $2\pi/(4\text{ mm}) \le k_x, k_y \le 2\pi/(2\text{ mm})$. An overall contrast of 1.35 is observed.

ACKNOWLEDGMENT

The author thanks Prof. G. Agrawal for his expert advice and direction, Dr. John Kelly for suggesting this project and the in-depth discussions that followed, and Dr. Stephen Craxton for many useful discussions and time spent editing this manuscript. This research was supported by NSF Grant PHY94-15583. In addition, this work was partially supported by the U.S. Department of Energy Office of Inertial Confinement Fusion under Cooperative Agreement No. DE-FC03-92SF19460, the University of Rochester, and the New York State Energy Research and Development Authority. The support of DOE does not constitute an endorsement by DOE of the views expressed in this article.

REFERENCES

1. K. Kato, unpublished (1984).

2. Laboratory for Laser Energetics LLE Review **45**, 1, NTIS document No. DOE/DP40200-149 (1990). Copies may be obtained from the National Technical Information Service, Springfield, VA 22161.

3. S. Skupsky, R. W. Short, T. Kessler, R. S. Craxton, S. Letzring, and J. M. Soures, J. Appl. Phys. **66**, 3456 (1989).

4. A. B. Carlson, *Communication Systems: An Introduction to Signals and Noise in Electrical Communication*, McGraw-Hill Electrical and Electronic Engineering Series (McGraw-Hill, New York, 1968), p. 154.

5. R. L. Sutherland, *Handbook of Nonlinear Optics*, Optical Engineering, Vol. 52 (Marcel Dekker, New York, 1996).

6. G. P. Agrawal, *Nonlinear Fiber Optics*, Optics and Photonics Series, 2nd ed. (Academic Press, San Diego, 1995).

7. Ts. Gantsog and R. Tanas, J. Mod. Opt. **38**, 1537 (1991).

8. K. E. Oughstun and G. C. Sherman, *Electromagnetic Pulse Propagation in Causal Dielectrics*, Springer Series on Wave Phenomena, Vol. 16 (Springer-Verlag, Berlin, 1994).

9. J. W. Goodman, *Introduction to Fourier Optics* (McGraw-Hill, New York, 1968).

10. R. W. Hellwarth, D. M. Pennington, and M. A. Henesian, Phys. Rev. A **41**, 2766 (1990).